Reef flat flow dynamics for a nearly closed fringing reef-lagoon: Ofu, American Samoa

Samantha A. Maticka[1,2], Justin.S. Rogers[1], C.Brock Woodson[3], Ben Hefner[3], and Stephen G. Monismith[1]

[1]The Bob and Norma Street Environmental Fluid Mechanics Laboratory, Department of Civil and Environmental Engineering, Stanford University, Stanford, CA, 94305-4020, USA

[2]Geosciences Montpellier, Université Montpellier, CNRS, Univ Antilles, Montpellier, France

[3]College of Engineering, University of Georgia, Athens, GA, 30602, USA

Key Points:

- Wave driven flows and flow dynamics vary with tidal water level
- Coral reef lagoon appears closed at high tide and open at low tide
- Flow structure for wave-driven flow resembles surf-zone when the lagoon is closed, and can be modeled using a wave-based eddy viscosity

Corresponding author: Stephen Monismith, `monismith@stanford.edu`

Abstract

We discuss observations of tidally varying wave-forced flows in the reef system on Ofu, American Samoa, a barrier reef and lagoon system that appears open at low tide and closed at high tide. At high tide, the free surface pressure gradient nearly balances the radiation stress gradient in the depth-integrated momentum equation. At depth, there is an imbalance between these two forces, generating an undertow and flows that turn alongshore and, for some of the time, offshore, behavior similar to rip currents observed on beaches. At low tides, the wave forcing drives purely onshore flows. In general, wave transport (including assumed roller behavior) is important to determining the total net transport. In both cases, the vertical structure of this flow can be predicted with some accuracy using the surf-zone model of Svendsen (1984), albeit with an eddy viscosity that is proportional to the rms wave velocity. While the dynamically closed nature of the lagoon mostly suppresses cross-reef transport, there is always some flow through the lagoon, with the strongest flows occurring at high tides and when the wave forcing is strongest.

Plain Language Summary

Waves and flows observed in the coral reef lagoon system located on the south shore of Ofu, American Samoa show that flows in the lagoon are driven by incident swell modulated by tidal variations in depth on the steep fore reef and on the shallow reef flat. At low tide, flows are across the reef flat from the fore-reef to the lagoon behave as though the lagoon is open to the ocean, whereas at high tide, flows into the lagoon are strongly limited by the resistance felt by the flow out of the lagoon. As a consequence, flows on the reef flat can develop an undertow, as is seen on beaches, although this varies with position on the reef flat. Nonetheless, overall flows in the lagoon are strongest at high tides and weakest at low tides.

1 Introduction

The wave-driven flow through fringing reef-lagoon systems is often described using a one dimensional model (Symonds et al., 1995; Coronado et al., 2007; Hearn, 1999; Hench et al., 2008; Lowe et al., 2009; Taebi et al., 2011; Monismith et al., 2013; Zhang et al., 2012; Sous et al., 2020), and has shown to be an important flushing mechanism for many reefs (Munk & Sargent, 1954; Callaghan et al., 2006; Davis et al., 2011; Symonds et al., 1995; Hearn, 1999; Hench et al., 2008; Lowe et al., 2009; Rogers et al., 2017), i.e., one that is important to determining the response to surface heating (Zhang et al., 2013), or the extent to which benthic communities can change bio-geochemical properties of lagoon waters (Koweek et al., 2015). In the 1D model, waves approach from offshore, shoal, steepen, and break near the reef crest, leading to a setup on the reef-flat that drives flow into the lagoon, and out through channels in the reef. The area on the fore-reef where waves break is referred to as the surf zone; the momentum balance there is between the pressure gradient force due to variations in the free-surface height and the radiation stress gradient. On the reef flat, the balance is generally assumed to be between the pressure gradient force and the bottom drag on the reef flat.

The strength of the wave-driven flow over the reef flat depends on the slope of the free-surface, and, thus on setup of the water level in the lagoon (Lowe et al., 2009). In what follows, a closed lagoon vs. open lagoon refers to how easily the incoming ocean water can leave a reef system, behavior that is determined by the geometry of channel openings (Gourlay, 1996). Using 2D simulations with different idealized geometries, Lowe et al. (2010) found that lagoon setup varied with the width of the outflow channel: Setup in the lagoon was larger for systems with narrow outflow channels, i.e., systems that were nearly closed. In this case, the flow was not one dimensional, but instead was similar to what is seen on beaches, i.e. rip currents as a mechanism for water returning to the ocean as opposed to flows out channels (Lowe et al., 2010). These simulations also show that the cross-reef transport is reduced, and can be redirected along the reef. Thus it appears that the 1D model best fits systems that have relatively large outlet channels, i.e., that appear to be *open*. These two limits might be exemplified by Kaneohe Bay as a closed system (e.g. Lowe et al. (2009)) and the reef on the north shore of Moorea as an open system (e.g. Monismith et al. (2013)).

Using theory and numerical models, Lindhart et al. (2021) investigated how the flow dynamics of an idealized version of the reef-lagoon system found on Ofu, American Samoa varied tidally. They found that depending on water level, the system could be considered either open or closed. They suggested that the extent to which reef systems should be classified as open or closed depends on the momentum balance operating on the reef flat as opposed to the geometry of the reef lagoon. They define open systems as ones exhibiting a balance on the reef flat between an onshore, wave-generated pressure gradient balanced by friction, and closed systems as ones for which the onshore radiation stress gradient is opposed by an offshore pressure gradient.

In the present paper, we use field observations made on Ofu, American Samoa in March 2017 to look in detail at the dynamics of flows on the reef flat for times when the Ofu reef-lagoon system appears open and times when it is closed. We consider below the relationship between setup and wave forcing (section 3.2), transports on the reef flat and in the lagoon (section 3.3), the depth and wave-averaged momentum balance (section 4.1), and the vertical structure of flows on the reef flat in light of the surfzone model of Svendsen (1984) (section 4.2). Rogers et al. (2018) describe the general conditions (tides, waves, etc.) observed during this experiment but focuses on the connection between the statistics of reef topography and frictional drag in the lagoon. In the present paper we focus on the behavior and dynamics of wave-driven flows on the reef flat, especially considering the extent to which the system is open or closed.

2 Field Site and Instrumentation

All of the measurements we report here were made in and near the reef lagoons on the south shore of Ofu, American Samoa (14.28S, 169.78W) (Fig. 1) from March 10-28, 2017. Ofu is almost entirely surrounded by a fringing reef extending ca. 100-200 m from the shore. The reef flat itself is about 100 m wide, which is significantly narrower than many other reef sites (Wiens et al., 1962; Hench et al., 2008; Lowe et al., 2009). The reef flat has a tidally-averaged depth of $\sim$0.5 m and has a fairly uniform coverage of roughness features on the order of 5-20 cm high, few of which are living coral. The associated lagoon is $\sim$2 m deep and has significant coral coverage with features that range from 5 cm to 2 m (Chirayath & Earle, 2016; Oliver & Palumbi, 2009). Physically, Ofu is a common fringing reef-lagoon system; i.e., the lagoon axis is parallel to shore and has channels through the reef to connect the lagoon to the ocean. However, compared to systems studied previously (e.g. (Hearn, 1999; Hench et al., 2008; Lowe et al., 2009; Coronado et al., 2007)), the Ofu reef system has only a few narrow channels as well as higher friction in the lagoon due to the large coral structures; thus, it is an excellent site for studying wave-driven flow dynamics of closed lagoons.

The field study employed instruments measuring velocities, pressures, and temperatures throughout the lagoon to observe spatial and temporal variability in both waves and mean flows on the fore-reef, in the lagoon and in the exit channel (pass). Figure 1 and Table 1 (see also Maticka (2019)) list the various instruments deployed throughout our 18 day experiment that will be discussed below, as well as their various sampling parameters. Beside the instruments shown in Fig. 1, a weather station was also situated on the beach c.a. 1.4 km SW from the field site.

In this paper we focus primarily on the behavior of waves and flows using data from instruments located along the cross-reef D-transect, sites starting with 'D', D-3, D-4, D-5, all situated on the reef flat, D0 in the lagoon, and FR5 and FR15 on the fore-reef. Along this transect the reef flat is $\sim 135m$ wide, and nearly flat with a slight increase in depth toward the lagoon ($dh/dx \approx 4{\times}10^{-3}m/m$). This line included RBR solo pressure loggers (accuracy = 1 cm; precision = 0.2 mm) except at FR15, where there was a Seabird SBE26+ wave/tide recorder (accuracy = 1 mm; precision $<$ 0.4 mm). At stations D0 and FR15, velocity and wave measurements were made with 2Mhz and 1Mhz Nortek Acoustic Doppler Profilers respectively.

Detailed velocity profiles on 3 s intervals were obtained at D-4 using a Teledyne RDI vADCP configured to run autonomously (Hefner et al., 2019). Unfortunately besides the failure of the vADCP after 5 days due to instrument flooding, the RBR pressure sensor deployed at D-4 also failed to record any data. Nonetheless, because of the unique data provided by the vADCP, the analysis below will primarily focus on those 5 days.

Finally, in addition to moored instruments, several releases of shallow GPS drifters constructed with radio-tracked dog collars (Herdman et al., 2015) were conducted in the lagoon for both high and low tide conditions to observe Lagrangian flows in the lagoon.

A key aspect of analyzing the behavior of flows in systems like the Ofu reef is removing wave signals, i.e., performing wave-averaging, which we will denote in all of what follows for any variable, f by $\overline{f}$. In analyzing our data we used three approaches for this averaging:
(1) Half hour averages of water levels: Wave statistics and mean water levels for all the pressure sensors were computed this way so as to match the half-hourly wave burst data acquired by the SBE26+ at station FR15.
(2) One hour averages of data acquired by the vADCP at station D-4. This was done to balance removal of variability associated with both waves and instrument noise with temporal resolution of the flow. This approach also facilitated separating wave and mean properties which could not be done using time series filtering except below the lowest depth (including both tides and waves) recorded at any time by the vADCP.

(3) Low pass filtering using a 4^{th} order Butterworth filter with a cutoff frequency of 0.5 cph to remove all waves and 0.042 Hz to separate infragravity and swell band waves. This pair of cutoff frequencies was used with the vADCP data to examine transport variability associated with wave-averaged flows, infragravity waves, and swell.

[Figure 1 about here.]

[Table 1 about here.]

3 Observations

3.1 Forcing

During this study, the forereef tidal range was ~1 m (Fig. 2 a), resulting in water depths on the reef flat ranging from ~ 35 cm to 1 m. The wind was weak, with speeds less than 5 m/s, and typically toward the West (positive cross- and negative alongshore components) (Fig. 2b). The wind-induced surface stress, τ_s was estimated with the commonly used quadratic drag law, $\tau_s = C_D \rho_{air} U_a |U_a|$, where $\rho_{air} = 1.23 kg/m^3$ is the density of air, $C_D = 0.0008$ is the drag coefficient for wind velocities less than 6.6 m/s (Hellerman, 1967), and U_a is the wind velocity. Thus, on average $\tau_s \simeq 0.005$ Pa, and had a maximum value of ca. 0.033 Pa. Thus, wind stresses were much smaller than the other measured forces on the reef flat (see below) and so will be neglected in the rest of what follows.

[Figure 2 about here.]

Figures 2 b and 2 c show: (a) the connection between wave forcing, calculated spectrally as in Monismith et al. (2015) using the pressure data at FR5 corrected for frequency-dependent attenuation, and setup between the fore-reef (FR15) and the ocean-ward edge of the reef flat (D-5); and, (b) the very small sea surface elevation difference across the reef flat (i.e, between D0 and D-5); The setups shown are calculated as the wave-averaged depths minus the average depth for the whole record, i.e., for any location

$$\bar{\eta}_* = h - \frac{1}{T_R} \int_0^{T_R} h dt \qquad (1)$$

where h is the the measured wave-averaged depth, and T_R is the length of the record. As will be discussed below, this approach also removes the mean setup, which must be found separately (see also Monismith et al. (2013)). As seen in Fig. 2, there is little cross-shore variation in mean sea surface height inshore of breaking; thus, as described by Lindhart et al. (2021), the Ofu lagoon appears to be "closed". The dynamics of the reef flat flows will be explored further below. Finally, as noted by Koweek et al. (2015), flows in the lagoon are in phase with tidal elevation and are clearly related to the strength of the wave forcing. Thus, the Ofu reef might be better described as "mostly closed" in that waves do force flows through the lagoon despite the high resistance associated with large roughness in the lagoon (see Rogers et al. (2018)) and the narrow exit channel between pools 400 and 500.

Wave forcing on the forereef consisted of longer-period (12-22 s) swell events and local short period (4-7 s) waves, with H_{rms} ranging from ∼0.4-1 m (Fig. 3), that broke normal to the crest (-0.8°±2.3°). Applying the approach of Sheremet et al. (2002) (their equations 2 and 3) to the FR15 ADP wave burst velocity and pressure data, we found that ca. 10 % of the sea-swell (SS) wave energy flux was reflected seaward off the forereef. Due to this relatively small amount of reflection and the near-normal wave direction on the reef, we assume in our analysis below that 100% of the energy flux is shoreward.

Offshore of the reef crest, virtually all of the wave energy was in the sea-swell band, whereas inshore of breaking, virtually all of the wave energy is in the infra-gravity wave band (Maticka, 2019) (see Supplementary material Fig S.1). On the reef flat itself, the bore-like waves were: (a) dissipated by bottom friction and continued breaking; and, (b) weakened by nonlinear transfers from high to low frequencies. By the end of the reef flat the bores had become transformed into trains of nonlinear solitary-like waves, i.e., there was rank ordering of waves in each wave train. The details of these transformations are discussed in Maticka (2019).

[Figure 3 about here.]

As is commonly found (e.g. Lowe et al. (2009)), waves on the reef flat varied with water level (Fig. 3 a,b), with $\sim 60\%$ reduction in H_{rms} from high tide to low tide. Evidently, for the Ofu reef, the majority of tidal variations in wave height take place on the shallow forereef where breaking occurs (Maticka (2019)). Unlike what is seen on beaches (e.g. Raubenheimer et al. (1996)), inshore of D-5, local wave height was not a constant fraction of the local depth (Fig. 3 b). This reflects the fact that bottom friction appears to be more important than depth-limited wave breaking for dissipating energy on the reef flat. Indeed, following Péquignet et al. (2011), we examined modeling dissipation due to wave breaking between D-5 and D-3 using the model of Battjes and Janssen (1978); unfortunately, dissipation computed using this method was uncorrelated with the dissipation estimated from the difference in shoreward wave energy flux. In contrast, the observed dissipation rate could be fit to the standard bottom friction model, $\epsilon = 0.6\rho f_w U_{rms}^3$, with a wave friction factor, $f_w = 0.34 \pm 0.002$ ($r^2 = 0.88$).

In addition to the depth-dependent wave-height reduction, incident gravity wave wave energy was transferred to both infragravity and far-infragravity bands (see also Péquignet et al. (2014)). Evidently, this infragravity wave forcing excites multiple resonant oscillations in the lagoon (Fig. 4), presumably at the natural frequencies of the lagoon (Maticka, 2019). These too vary tidally in both strength and, because of large relative variations in lagoon depth, period. We note that the infragravity wave behavior seen on Ofu has also been observed on the Ouano barrier reef system (Sous et al., 2019).

[Figure 4 about here.]

3.2 Free Surface Response to Waves

The setup or setdown of the free surface relative to offshore, $\overline{\eta}_r$ represents the wave-averaged effect of wave forcing on the free-surface (Longuet-Higgins & Stewart, 1964; Mei et al., 1989). As shown by Vetter et al. (2010), this setup depends on the incident wave energy flux, F, the depth on the reef flat, h_r, and the breaking depth fraction for depth-limited breaking, γ,*viz*,

$$\overline{\eta}_r \simeq \frac{3\gamma^2}{8+3\gamma^2}\left(\frac{(8F_w/\rho)^{2/5}}{g^{3/5}\gamma^{4/5}} - h_r\right) \tag{2}$$

Thus, per eq.2 the amount of setup may vary with the tides due to tidally modulated breaking (Callaghan et al., 2006): As the water level decreases, setup on the reef increases. Per eq. 2, there will be a limiting value of F for a given value of h_r for which there is no breaking and hence no setup. Generally γ depends on the geometry of the reef, i.e., fore-reef steepness (Raubenheimer et al., 1996) and the presence or absence of a reef crest ridge (Yao et al., 2012); thus, at present γ should be viewed as a free parameter to be determined from observations.

[Figure 5 about here.]

In the present case, we defined $\overline{\eta}_r$ as the difference in wave-averaged sea level height between the fore-reef and the first reef flat station, i.e., $\overline{\eta}_{D-5} - \overline{\eta}_{FR15}$. Computing setups using eq.1 removes any mean differences in elevation between the pressure sensors, but also removes the mean setup. Thus, there is an offset that must be determined using additional information. Based on eq. 2, the depth of no setup can be estimated by plotting $\Delta\overline{\eta}_{r*} = \overline{\eta}_{D-5*} - \overline{\eta}_{FR5*}$ as a function of F and forereef depth. Doing so, we find that the offset between FR5 and D-5 is $\simeq$ 12 cm (see Supplementary material Fig S.2), i.e., $\Delta\overline{\eta}_r = \Delta\overline{\eta}_{r*}+0.12$. Predicted and observed setup time series using this value, and $\gamma = 0.87$ and h_r varying tidally with a minimum depth of 0.25 m are shown in Fig. 5.

Setup calculated on the reef flat (D-5) was generally consistent with predictions made using eq. 2, where $\overline{\eta}_r$ increases with wave energy flux, and decreases with reef depth as a result of tidally-modulated wave breaking (Fig. 5c). The error in model predictions (figures 5 d and e) was generally small, except near low and high water. Arguably this reflects changes in breaking dynamics; in principle, γ could be made a function of forereef depth to better match the observations, but this would not likely have much generality and so would not be particularly useful. Nonetheless, the value of γ found here is similar to that found by Monismith et al. (2013) for the Moorea forereef (0.98).

Setup in the lagoon (D0) followed the same trend, with little difference in free surface elevation between the reef flat and the lagoon (Fig. 2d). This is the behavior that is expected for a closed lagoon (Gourlay, 1996; Lowe et al., 2010), i.e., a nearly spatially-uniform setup in the cross-shore direction. In contrast, the free surface height in an open lagoon will be equal to that of the offshore ocean (Symonds et al., 1995). Evidently, for the case of Ofu, the combination of high friction in the lagoon (Rogers et al., 2018) and the narrowness of the exit channel relative to the overall alongshore length of the lagoon (20 m vs ca. 500 m) combine to create a relatively closed system.

[Figure 6 about here.]

3.3 Flows on the Reef Flat

While the difference in setup between the reef flat and the lagoon was small, there was flow across and along the reef flat (fig. 6).The cross-reef flows were strongly sheared, with offshore flows near the bottom at high tide early in the record, and over nearly all of the depth at high tides in the later part of the record. Throughout the record, flows were onshore at low tides. The transition between these two conditions took place near when $\overline{\eta} \simeq 0$. In contrast to the strongly sheared cross-reef flows, the alongshore flows were nearly unsheared and were primarily directed towards the channel to the northeast.

The volumetric flux per unit width (transport), $\overline{q}(t)$ was calculated by integrating the V-ADCP velocity profiles $(U_x(z,t), U_y(z,t)))$ over depth using the assumption that the velocity was zero at the bed $(z = 0)$. Thus, the wave-averaged flow is given as:

$$(\overline{q}_x, \overline{q}_y) = \overline{\int_0^{h+\eta(t)} (U_x, U_y) dz} \tag{3}$$

The transport in the lagoon was mostly directed alongshore and had a strong tidal variation, but with a magnitude that was dependent on the strength of the wave forcing on the forereef (Fig. 2e). On the reef flat, the vADCP resolved approximately 90% of instantaneous depth. Thus, because the averaging was applied to the instantaneous transport, the computed wave-averaged flows (shown here for the x direction) include both the mean Eulerian transport, $\overline{q}_{x,E}$ and the wave transport, $\overline{q}_{x,W}$, i.e., the time-averaged transport due to waves (Monismith et al., 2013). This decomposition conventionally involves writing

$$\overline{q}_{x,E} = \int_0^{\overline{h)}} \overline{U}_x dz \tag{4}$$

and

$$\overline{q}_{x,W} = \overline{q}_x - \overline{q}_{x,E} \tag{5}$$

which is equivalent to averaging the instantaneous wave transport.

Potential issues with computing the wave transport using the vADCP data are: (1) the relatively low sampling frequency of the vADCP; (2) the fact that depth for the vADCP was measured using surface tracking; and (3) the inability of the instrument to measure velocities in the upper-most 10% of the water column. The low time resolution means that the swell-band waves were not fully resolved, potentially causing the wave transport computed per eq. 5 to be smaller than the actual value. The use of surface tracking rather than pressure to measure the instantaneous depth likely results in increased noise in the surface elevation time series. Lastly, the missing near-surface region is where surface rollers form (Svendsen (1984)), and so the vADCP-measured transport likely does not include transport associated with the rollers.

One way to assess the ability of the vADCP to accurately measure the wave-induced velocity is to look at the velocity data in light of shallow water theory which gives the instantaneous wave-induced velocity (which is independent of depth), $\tilde{U}_x$ as a function of the instantaneous free-surface deflection $\tilde{\eta}$ and mean depth, h,

$$\tilde{U}_x = \frac{\tilde{\eta}\sqrt{gh}}{h} \tag{6}$$

or equivalently

$$\tilde{U}_{x,rms} = \sqrt{\overline{\tilde{U}_x^2}} = \frac{\sqrt{\overline{\tilde{\eta}^2}}\sqrt{gh}}{h} = \frac{\eta_{rms}\sqrt{gh}}{h} \tag{7}$$

In terms of transport, eq. 6 implies that

$$\overline{q}_{x,W} = \frac{\eta_{rms}^2\sqrt{gh}}{h} \tag{8}$$

Whereas eq. 7 provides a good description of the vADCP velocities, the measured instantaneous velocities are poorly correlated with and significantly less than theoretical values (see Supplementary figure S.2). As a consequence, the computed wave transports are significantly less than what would be calculated using 8.

The closest instrument to the vADCP that should properly resolve wave motions, and thus can be used to test eq. 8, is the ADP at D0. In this case, the observed wave transports were 40% of what would be predicted by eq. 8 ($r^2 = 0.78$) As seen in the vADCP data, velocities more closely matched theory, with eq. 7 applies with a constant of 0.84 rather than 1 ($r^2 = 0.82$). Moreover, η_{rms} at D-4 inferred from surface tracking matches well values of η_{rms} that would be estimated by interpolation of values of η_{rms} between D-5 and D-3. Thus, while the vADCP surface tracking may have resolved most of the surface wave variance, it did not properly resolve the wave transport, possibly an effect of noise. Thus, in the absence of any better estimate, we computed the non-roller portion of the wave transport at D-4 using measured values of η_{rms} and eq. 7 multiplied by 0.4. To include the additional transport associated with the presumably unresolved rollers, we supplemented this estimate with an estimate of the roller transport based on eq. 2.10 in Svendsen (1984):

$$q_R = 0.9\frac{H_{rms}^2}{T} \tag{9}$$

where H_{rms} is the rms wave height, and T is the wave period.

[Figure 7 about here.]

Figure 7 shows that instantaneous flows associated with the waves on the reef flat were roughly an order of magnitude larger than the wave-averaged flows, with swell band and infragravity wave band flows being comparable to each other. Despite the fact that the instantaneous flows were wave dominated, the portion of the estimated wave transport on the reef flat described by eq. 8 appears to have been much less than the mean Eulerian transport, behavior also reported for broken waves on Moorea by Monismith et al. (2013). On the other hand, for much of the record, the roller transport may have been significant. Overall, there was a striking reversal of the wave-averaged cross-reef Eulerian flow such that during the latter part of the record shown in Fig. 7, flow was nearly directed offshore at times. This behavior will be discussed further below in the context of the dynamics of flows on the reef flat. While it is strikingly different from what has been reported for other barrier reefs, the appearance of an "undertow", i.e. an offshore directed Eulerian mean flow is something that is commonly seen on beaches. Thus, as reflected by the behavior of the mean water levels on the reef flat and in the lagoon, Ofu appears to be mostly closed, i.e., beach-like. Another distinctive feature of flows on the Ofu reef flat is that the along reef flow is comparable to the cross-reef flow such that at high tides, flow on the reef flat is directed towards the channel between pools 400 and 500 rather than either onshore or offshore. As a result, the flow direction alternates between primarily cross-shore at low tide and primarily alongshore at high tide.

In addition to the vADCP observation of undertow, Lagrangian drifter tracks (see Maticka (2019)) show that besides the main channel, offshore flows were also consistently present near station H-1, behavior seen in the vADCP data taken there and discussed in (Hefner et al., 2019). However, at high tides, offshore flows also appeared near the D-transect, behavior that is similar to rip currents that develop on beaches (MacMahan et al., 2006) (see fig. 1 in Rogers et al. (2018)). For the Ofu reef, the fact that outflows take place at consistent locations other than in the main channel may reflect the way small variations in reef crest topography can support relatively stable, but tidally variable, plan-form variable currents. On the other hand, for low tides, flows were towards and out of the channel, conditions seen in other, more "open" systems (Symonds et al., 1995; Hench et al., 2008).

In summary, the flows we observed at high tide differed from what would be expected of the simple 1D model and are consistent with predictions from numerical simulations of closed reef-lagoon systems, for which rip currents and along-reef flows might be expected (Lowe et al., 2010). Additionally, we observed an undertow, something not captured in the simulations of Lowe et al. (2010) since their model did not resolve the vertical flow structure. In contrast, the low tide conditions are consistent with the standard 1D conceptual model of wave-driven flows, i.e., there is flow shore-ward over the reef flat, then along the lagoon towards the channel, and then out the exit channel.

4 Momentum Balance on the Reef Flat

Due to the narrowness of the Ofu reef flat (ca. 100 m) the incident waves, while broken, were not fully dissipated by the time they reached the reef flat stations (D-5, D-4, D-3). As the water level decreased with the tide, the fraction of waves that broke on the forereef increased, which decreased wave height and energy on the reef flat, but increased the amount of setup on the reef flat. As the water level rose and waves prevailed on the flat, the velocity profiles changed from onshore over the depth to onshore near the surface and offshore near the bed. To explain the depth-dependent flow dynamics, we first consider the depth-integrated momentum balance of the cross-reef flow, and then consider the dynamics of the vertical shear in light of the undertow model of Svendsen (1984). These analyses will be done for the section of the reef flat between D-5 and D-3, using the vADCP measurements at D-4.

4.1 Depth-integrated momentum balance

The cross-shore component of the 1D steady, wave-averaged, depth-integrated momentum equation commonly used to describe nearshore flows is (Mei et al., 1989):

$$\frac{d}{dx}\left(\frac{\overline{q}_x^2}{h+\overline{\eta}}\right) = -g(h+\overline{\eta})\frac{d\overline{\eta}}{dx} - \frac{1}{\rho}\frac{dS_{xx}}{dx} - \frac{1}{\rho}\frac{dR}{dx} - \frac{\tau_b}{\rho} \tag{10}$$

x is the principal flow direction (i.e, cross-reef), h is water depth, $\overline{\eta}$ is time-averaged free-surface height deviation from mean sea level, τ_b is the bottom stress, S_{xx} is radiation stress due to waves (calculated spectrally), and R is the extra contribution to the wave forcing due to the presence of surface rollers (Svendsen, 1984). From left to right the terms in eq. 10 will be referred to as advection (ADV), pressure gradient force (PGF), radiation stress gradient (RSG), roller force (RF), and bottom friction (BF). It is important to note that the flow appearing in Eqn. 10 is the total flow q, i.e. the flow including both Eulerian and wave transports (Monismith et al., 2013).

Advection is often not important in reef-lagoon systems (Sous et al., 2020). For the reef flat at Ofu: $\overline{q} \approx 0.05m^2/s$, $h \approx 0.5m$, $dq/dx \approx 0$ (from 1D continuity), $dh/dx \approx -4x10^{-3}m/m$ (see Maticka (2019)), and $\overline{\eta} << h$. Thus, we estimate:

$$\frac{d}{dx}\left(\frac{\overline{q}_x^2}{h}\right) = \frac{2\overline{q}_x}{h}\frac{d\overline{q}_x}{dx} - \frac{\overline{q}_x^2}{h^2}\frac{dh}{dx} = -\frac{\overline{q}_x^2}{h^2}\frac{dh}{dx} \approx 4x10^{-5}\frac{Pa}{kg/m^3} \tag{11}$$

For most of our study period, this is 1 to 2 orders of magnitude smaller than our estimates for the other forces. As with wind stresses, advective accelerations are neglected in what follows, although it may be important in times when the flow transitions to a horizontally varying flow.

Thus, neglecting advection, we write eq. 10 as

$$-\frac{1}{\rho}\frac{dS_{xx}}{dx} - \frac{1}{\rho}\frac{dR}{dx} = g(h+\overline{\eta})\frac{d\overline{\eta}}{dx} + \frac{\tau_b}{\rho} \tag{12}$$

where then LHS represents the wave forcing, and the RHS represents the possible response. For reef flats in open systems, both the RHS and LHS are zero, i.e., the wave forcing is nearly zero and the pressure gradient across the reef balances bottom drag (c.f. the Moorea reef - Monismith et al. (2013)), whereas for closed systems, e.g. beaches, the wave forcing is balanced by the pressure gradient, and the flow and thus the bottom drag are small. We will consider each of the terms in eq. 12 in turn below.

RSG $(-dS_{xx}/dx)$ is calculated using finite differences as $-dS_{xx}/dx \simeq -\Delta S_{xx}/\Delta x$ where Δx is the cross-shore distance from D-5 to D-3. ΔS_{xx} was calculated by differencing the results of spectral integration of the wave data at D-5 and D-3 including both the sea & swell and the infragravity frequency bands (f_1-f_2=0.004-0.25Hz):

$$S_{xx} = \rho g \int_{f_1}^{f^2} P_{\eta\eta}(f,t) \cdot \left(2\frac{C_g}{C} - \frac{1}{2}\right) df \tag{13}$$

Here f is the frequency, t is time, C_g is wave group velocity, C is wave phase speed, and $P_{\eta\eta}$ is the spectral density of variations in the free surface height modified to account for frequency-dependent attenuation of the pressure. The roller force was calculated following Fredsøe and Deigard (1992) as:

$$R \simeq 0.9\rho\frac{H_{rms}^2 C}{T} \tag{14}$$

where $C = \sqrt{gh}$.

While the wave forcing can be calculated explicitly, the PGF and BF terms both include parameters that are unknown *a priori*. The free-surface slope on the reef flat shown in Fig. 2 does not include whatever mean setup might have existed during our field experiment. If a quadratic drag law is used, then the drag coefficient, C_D, must also be determined in some fashion. In what follows, we will pursue an iterative approach to estimate both the unknown mean setup and C_D.

The 1D wave-averaged quadratic drag law

$$\overline{\tau_b} = \rho C_D \overline{U_x (U_x^2 + U_y^2)^{1/2}} \tag{15}$$

is often used to represent bottom stress (Grant & Madsen, 1979; Lentz et al., 2017), where (U_x,U_y) is the depth- averaged Eulerian velocity, and C_D is the drag coefficient. When waves are present, the velocities appearing in eq. 15 include both wave averaged velocities and the wave velocities, i.e. $U_x = \overline{U}_x + \tilde{U}_x$ (Feddersen et al., 2000). Thus, the bottom drag acting in the x direction will be

$$\overline{\tau_b} = \rho C_D \overline{(\overline{U}_x + \tilde{U}_x)|\overline{V} + \tilde{V}|} \tag{16}$$

where $V = (U_x^2 + U_y^2)^{1/2}$. If $\tilde{V}_{rms} >> \overline{U}_x$, then $\overline{\tau_b} \simeq 2\rho C_D \overline{U}_x \tilde{V}_{rms}$ (Wright & Thompson, 1983).

[Figure 8 about here.]

For the surface slope, we started with the difference in $\overline{\eta}_*$ (defined by eq.1) between D-2 and D-5 (60 m separation) rather than between D-3 and D-5. The reason for using these two stations rather than the pair D-3 and D-5 to estimate $\frac{d\overline{\eta}}{dx}$ was that the PGF calculated using D-3 and D-5 (30 m separation) tended to be too noisy. Note that the sea level differences are on par with the stated accuracy of the pressure sensors (ca. 1 cm) but are still somewhat greater than the stated resolution of the sensors (0.2 mm).

Estimates of both the setup offset and C_D were found by trial and error iteration. To do this we computed the lack of closure in the momentum balance, i.e., the error E, as:

$$E = PGF + BF - (RSG + RF) \tag{17}$$

This iteration was carried out by first choosing a value of C_D, and then finding the offset in setup and C_D that produced a mean value of $E \simeq 0$. The iteration proceeded by choosing different values of C_D and repeating this process, with the goal of making

E_{rms} as small as possible and so that a linear fit of $(PGF+D)$ as a function of $(RSG+RF)$, should give a slope $\simeq 1$. Following this procedure we found that the setup adjustment between D-2 and D-5 $\simeq$ 7.6 mm upwards, and that $C_D \simeq 0.031$. The resulting force time series are shown in Fig.8. These parameters resulted in $(PGF + D) = (1 \pm 0.01)(RSG+RF)$ ($r^2 = 0.88$), and gave a mean error of 0.004 Pa and an rms error of 0.15 Pa (see Fig. 8e). One key feature of the momentum balance is that waves on the reef flat were always important to the drag (Fig. 8c), such that drag was well described by the linear model of Wright & Thompson (1983).

For the entire experiment (Fig. 8d), at high tides, the PGF was directed *offshore* and nearly balanced the wave forcing $(RSG+RF)$, behavior that is typically observed in surf zones on beaches (Longuet-Higgins & Stewart, 1964; Symonds et al., 1995), i.e., from the standpoint of the momentum balance, the Ofu reef is closed at high tide. In contrast, at low tides, the wave forcing was primarily balanced by bottom friction (BF), behavior characteristic of open reef systems, although in some cases (e.g., Hench et al. (2008)) the wave forcing is unimportant and instead $PGF \simeq BF$. Thus, the Ofu reef behaves as either a closed or open system depending on tidal water level. This behavior can be visualized using the force-balance ”phase plane” shown in Lindhart et al. (2021). As seen in Fig. 9, for water levels less than mean sea level, $RSG + RF$ tends to be $\simeq BF$, although unlike what is seen in model results shown in Lindhart et al. (2021), the PGF contributes to the force balance even at the lowest water levels. For water levels somewhat greater than mean sea level, $RSG + RF \simeq PGF$, although in this case the BF still plays a small role in the force balance.

[Figure 9 about here.]

The value of C_D we found on the reef flat is an order of magnitude larger than what is typically found for smoother surfaces like sandy bottoms on the inner shelf, i.e., ca. 0.003. This is plausible given the small-scale topography of the reef that varied between nearly flat to including corals that were ca. 10 cm high (Fig. 10). This value of C_D is within the (wide) range of drag coefficients reported for reefs, which vary from 0.009 to 0.8 (Rosman & Hench, 2011). Using the law of the wall (Pope, 2000), Lentz et al. (2017) showed that in some cases, variations in water depth could explain variability in C_D based on depth-averaged velocities. To test for this possibility, we considered an alternative to using a single value of C_D: Choose $C_D(t)$ so the momentum balance was satisfied for each time. Following this approach, we found no systematic variation of C_D with depth. Why this might be the case is that the observed velocity profiles (shown below) often cannot be described by the law of the wall, a likely effect of the vertical structure of the forcing. We tried using the near-bottom cross-reef velocity to parameterize drag, but doing so resulted in errors that were consistently larger than what was obtained using the depth-averaged velocity, and so are not presented here.

[Figure 10 about here.]

4.2 Vertical Structure of Reef Flat Flows

The vertical structure of flows in the surfzone is determined by the local force imbalance that arises because the RSG varies with depth, with the majority of the wave contribution to momentum flux occurring between the trough and crest (Svendsen, 1984). In particular, when waves are actively breaking, there is a surface roller that effectively imposes a shear stress on the underlying fluid. In contrast, because it is due to a sloping free surface, the PGF is constant over depth and, if it is directed offshore, produces an offshore flow near the bottom, i.e., an undertow. In the present case, what is important is that the RSG covaries with the tidal elevation (Fig. 8), producing a larger imbalance between the PGF and RSG throughout the water column at high tide, thus leading to stronger undertow.

The vertical structure of the reef flat flow can be examined using Svendsen's (1984) model for the mean Eulerian flow in surfzones. The local momentum equation valid below the wave trough (his eq. 4.1) reads

$$\frac{\partial}{\partial z}\left(\nu_t \frac{\partial \overline{U}_x}{\partial z}\right) = \frac{\partial \overline{U_{xw}^2}}{\partial x} + g\frac{\partial \bar{\eta}}{\partial x} \tag{18}$$

Thus

$$\frac{\partial}{\partial z}\left(\nu_t \frac{\partial \overline{U}_x}{\partial z}\right) = \frac{\partial \overline{U_{xw}^2}}{\partial x} - \frac{1}{\rho h}\frac{\partial S_{xx}}{\partial x} - \frac{\tau_b}{\rho h} \tag{19}$$

Note that S_{xx} includes the roller contribution, R (eq. 14), as well as what would be computed using linear theory, i.e., for shallow water waves

$$S_{xx} = \frac{3}{2}\rho g \eta_{rms}^2 + R \tag{20}$$

In analyzing our data, we used eq. 13, rather the simpler approximation eq. 20, to calculate S_{xx}, although the two sets of values are quite close. Assuming that the waves propagate in the x direction, and using shallow water theory to compute $\overline{U_{xw}^2}$ (eq. 7), then

:

$$\frac{\partial}{\partial z}\left(\nu_t \frac{\partial \overline{U}_x}{\partial z}\right) = -\frac{g}{2h}\frac{\partial \eta_{rms}^2}{\partial x} - \frac{1}{\rho h}\frac{\partial R}{\partial x} - \frac{\tau_b}{\rho h} = a\left(x\right) - \frac{\tau_b}{\rho h} \tag{21}$$

Including the bottom boundary condition on the stress, integration twice with respect to z gives:

$$\overline{U}_x = \int_0^z \frac{a\left(x\right)\xi + \left(\tau_b/\rho\right)\left(1-\xi/h\right)}{\nu_t\left(\xi\right)} d\xi + c\left(x\right) \tag{22}$$

The bottom kinematic boundary condition gives:

$$\overline{U}_x(0) = U_0 \Rightarrow c\left(x\right) = U_0 \tag{23}$$

with U_0 equal to the velocity near the bottom. This will be specified later. A common model for eddy viscosity in shallow flows is the parabolic distribution

$$\nu_t = \kappa u_* z\left(1 - z/h\right) \tag{24}$$

where u_* is the bottom friction velocity, although in the present case, this may not be the correct velocity scale. As an alternative, we re-write this as

$$\nu_t = \nu_0\left(z/h\right)\left(1 - z/h\right) \tag{25}$$

where ν_0 is expected to be a function of the strength of turbulence produced by wave breaking and by bottom boundary layer turbulence also associated with the waves. Thus

$$\overline{U}_x = -\frac{h}{\nu_0}\frac{\partial F}{\partial x}\int_{\frac{z_0}{h}}^{\zeta} \frac{1}{\left(1-\sigma\right)} d\sigma + \left(\frac{\tau_b h}{p\nu_0}\right)\int_{\frac{z_0}{h}}^{\zeta} \frac{d\sigma}{\sigma} = A\log\left(\frac{h-z}{h-z_0}\right) + B\log\left(\frac{z}{z_0}\right) \tag{26}$$

where $\sigma = z/h$ and, to make the integrations finite, we have replaced the lower limit with the dimensionless roughness length $\frac{z_0}{h}$, as is customary for turbulent channel flows. In principle, a similar adjustment would be needed near $z = h$. The radiation stress/forcing imbalance is

$$F = g\frac{\overline{\eta'^2}}{2} + \frac{R}{\rho} \tag{27}$$

and the two constants are

$$A = \frac{h}{\nu_0}\frac{\partial F}{\partial x} \quad B = \frac{\tau_b h}{\rho\nu_0} \tag{28}$$

Hence, one parameter to be determined by matching theory to observations is ν_0 and the other is U_0. In the absence of some form of turbulence closure that explicitly accounts for wave breaking and wave turbulence interactions, a simpler approach is to assume that that ν_0 is the product of suitable velocity and length scales, i.e.,

$$\nu_0 = \alpha\, U_{rms} h \tag{29}$$

where U_{rms} is the rms wave-induced velocity. By trial and error we found that $\alpha \simeq 0.5$ produced velocity profiles that best matched observed vertical shears. For U_0, there are several possibilities. Svendsen (1984) suggests that U_0 could be estimated from bottom boundary layer streaming. Alternatively, U_0 could be set equal to 0. A third possibility is that U_0 can be determined by requiring that the mean Eulerian transport calculated by the model is the same as that observed. Given the limitations of our data, we chose this last approach to evaluate U_0.

[Figure 11 about here.]

A comparison of theory and observations is shown in Fig. 11 for 4 profiles with the strongest flows into the lagoon (a-d) and 4 flows with the strongest undertows (e-h). Evidently, Svendsen's theory does a reasonable job in predicting the structure of the flow, although in the cases with strong onshore flow, the shear is stronger near the bottom and near the surface than theory would predict, suggesting that eq. 25 may not always be an appropriate description of breaking wave turbulence on the reef flat. Likewise, the interior of the water column is less sheared than the model predicts for the cases with strong undertows (i.e., offshore flows), suggesting that eq. 25 underpredicts the eddy viscosity in those cases. Finally, in nearly all cases, the near surface shear is stronger than predicted, behavior that may reflect the fact that on average, the uppermost part of the water column resolved by the vADCP may have been in the roller and so the basic model, eq. 18, is not strictly applicable there.

In summary, the surf zone flow model of Svendsen (1984) supplemented by a simple turbulence model provides a plausible description of the structure of flows on the Ofu reef flat. However, its predictive power is limited by the necessity of choosing an appropriate bottom boundary condition on the velocity, and by the complexity of turbulent flows with energetic broken waves, most notably near the surface in the roller produced by breaking. The vADCP measurements we present here were not designed to characterize the surf zone flow near the water surface or near the bottom, nor did we have available turbulence measurements that might enable us to better estimate bottom stresses and eddy viscosities. Given that reef flats with broken waves are a common feature of reefs and that flows there are important to wave runup and overtopping (Storlazzi et al., 2018), future efforts to examine this flow in more detail seem warranted.

5 Discussion and Conclusions

The Ofu reef appears to function as a (nearly) closed system at high tide, i.e., the offshore directed pressure gradient (PGF) balances the onshore directed wave forcing (RSG+RF) whereas at low tide, it appears open in that the wave forcing is balanced by bottom drag (BF). At high tide, the Ofu reef flat is similar to surf zones on beaches. In this case, the *offshore* direction of the PGF reflects the fact that as the depth on the reef flat increased with the tide, the strength of the wave forcing on the reef flat increased, although the wave-forced free-surface setup between the fore-reef and reef flat decreased. Nonetheless, at all times the wave-driven setup in the lagoon and on the reef flat were nearly the same and so the cross-shore pressure gradient on the reef flat was always much smaller than the pressure gradient in the region near the reef crest where waves first break.

The remarkable vertical resolution of the vADCP allowed us to observe how the variation of wave forcing with water level affected the vertical structure of the flow on the reef flat: As first described by Svendsen (1984), the depth variable difference between the RSG and PGF creates a vertically sheared flow with an undertow that reduces the depth-integrated cross-reef onshore transport (Svendsen (1984)). In effect, the flow structure at high tide (Fig. 11e-h) resembles a Poiseuille-Couette flow (Kundu et al. (2008)) with the surface stress directed onshore and the pressure gradient directed offshore. At low tide the combined effects of the vertically variable wave forcing and the PGF both acting to force fluid onshore; thus, flows at low tide were more like Couette flows (Fig. 11a-d). Using a parabolic eddy viscosity model in which the velocity scale was the rms wave velocity and not the shear velocity defined by the bottom stress, and choosing the bottom velocity boundary condition so as to match the total mean Eulerian transport, the vertical structure model of Svendsen (1984) could be fit well to the observed velocity profiles.

Although not directly measured, bottom stresses also appeared to be dynamically important when $\overline{q}_{x,E}$ was directed onshore. More importantly, given the vertical structure of the flow, it is hard to gauge the accuracy or generality of the value of C_D we derived based on closing the momentum balance. Clearly, future studies of reef flat dynamics should include direct measurements of bottom stresses if at all possible.

Wave-driven flows through the Ofu reef system were strongly modulated by the tides, with the strongest flows in the lagoon observed at high tides although even for the lowest tides, there is flow through the system. In contrast, the situation on the reef flat was more complicated. First, the cross-shore wave transport due to both shallow water wave dynamics and due to transport in the roller was always onshore whereas $\overline{q}_{x,E}$ recorded by the vADCP was directed onshore for part of the record and offshore for part of the record. Thus, the wave transport which we could only estimate rather than directly measure, was crucial to sustaining onshore flows. Secondly, for higher tides the principal direction of transport was directed nearly along the reef, rather than across the reef. This rotation is consistent with flow behavior seen in numerical simulations by Lowe et al. (2010) and Lindhart et al. (2021) for closed lagoon systems; it is not seen in open systems (e.g., John Brewer Reef - (Symonds et al., 1995) or Moorea - (Monismith et al., 2013)). However, the presence of outflows on the reef flat near sta. H-1 (the vADCP data shown in Hefner et al. (2019)), suggests that for closed systems, shallow outflow channels may develop where the reef crest is locally lower than adjacent sections. Whether or not these depressions could ultimately develop into "full fledged" channels is an open question.

Tidal modulation of flows through the Ofu lagoon also affects residence times

$$T_r(t) = L/\overline{U}_r(t), \tag{30}$$

i.e., the time a given water parcel spends in the lagoon after being transported onshore from the ocean corresponding to high tides. Here $L \simeq 600$ m is the approximate alongshore extent of pool 400, and $\overline{U}_r$ is a representative velocity for flow through the lagoon, in this case the depth- and wave-averaged alongshore velocity at D0. The strength of the modulation, as shown in Fig. 2, appears to have been about a factor of 3 for the ratio of largest to smallest values of T_r, as defined by the 5 % and 95% percentiles of T_r. Strikingly, T_r depended more strongly on water depth than on wave forcing strength (Fig. 12) during our two week experiment. It should be recognized that eq. 30 is only intended to represent a scale for the residence time, since in reality, water parcels that enter the lagoon near the channel will spend much less time in the system than do those that enter near the pool 300/400 separation line. Nonetheless, given that drifter observations suggest that T_r was ca. 1 hr at high tide (Maticka, 2019), the estimates given in Fig. 12 are reasonable approximations to the average behavior of the system.

[Figure 12 about here.]

Finally, one feature of the flows on reefs like the Ofu reef that deserves more consideration in future is the presence of relatively strong infra-gravity waves. Low-frequency variability of reef flat flows was comparable to swell-band variability, and water level fluctuations inside the lagoon showed the presence of multiple resonant modes, behavior also seen on the reef flat on Ipan, which also appears to be "closed" (Péquignet et al., 2009)). This is different from what was observed for flows and water levels on the much more open reef found on Moorea (Monismith et al. (2013)), suggesting that active infragravity wave fields are also an important characteristic of closed systems.

Acknowledgments

The authors are grateful for support of this work by the National Science Foundation through grants OCE-1536502, OCE-1536618, OCE-1736668, and OCE-1948189. We also thank Pago Pago Marine Charters, Annie Adelson and Emma Reid for their help with the 2017 field work. Finally, this work was conducted under permits from the U.S. Department of the Interior National Park Service, National Park of American Samoa, and the American Samoa Department of Marine and Wildlife Resources. The processed data discussed in this paper will be made available through the Stanford Digital Repository (https://purl.stanford.edu/) via a URL of the form https://purl.stanford.edu/file$_identifier$

References

Battjes, J. A., & Janssen, J. (1978). Energy loss and set-up due to breaking of random waves. In *Coastal engineering 1978* (pp. 569–587). ASCE.

Callaghan, D. P., Nielsen, P., Cartwright, N., Gourlay, M. R., & Baldock, T. E. (2006). Atoll lagoon flushing forced by waves. *Coastal Engineering*, *53*(8), 691–704.

Chirayath, V., & Earle, S. A. (2016). Drones that see through waves–preliminary results from airborne fluid lensing for centimetre-scale aquatic conservation. *Aquatic Conservation: Marine and Freshwater Ecosystems*, *26*, 237–250.

Coronado, C., Candela, J., Iglesias-Prieto, R., Sheinbaum, J., López, M., & Ocampo-Torres, F. (2007). On the circulation in the puerto morelos fringing reef lagoon. *Coral Reefs*, *26*(1), 149–163.

Davis, K., Lentz, S., Pineda, J., Farrar, J., Starczak, V., & Churchill, J. (2011). Observations of the thermal environment on red sea platform reefs: a heat budget analysis. *Coral Reefs*, *30*(1), 25–36.

Feddersen, F., Guza, R., Elgar, S., & Herbers, T. (2000). Velocity moments in alongshore bottom stress parameterizations. *Journal of Geophysical Research: Oceans*, *105*(C4), 8673–8686.

Fredsøe, J., & Deigard, R. (1992). *Mechanics of coastal sediment transport, advanced series on ocean engineering 3.* World Scientific.

Gourlay, M. (1996). Wave set-up on coral reefs. 1. set-up and wave-generated flow on an idealised two dimensional horizontal reef. *Coastal Engineering*, *27*(3-4), 161–193.

Grant, W. D., & Madsen, O. S. (1979). Combined wave and current interaction with a rough bottom. *Journal of Geophysical Research: Oceans*, *84*(C4), 1797–1808.

Hearn, C. J. (1999). Wave-breaking hydrodynamics within coral reef systems and the effect of changing relative sea level. *Journal of Geophysical Research: Oceans*, *104*(C12), 30007–30019.

Hefner, J. S., Brian B.and Rogers, Maticka, a. M. S. G., Samantha A, & Woodson, C. B. (2019). Instrumentation for direct measurements of wave-driven flow over a fringing reef crest. *Limnology and Oceanography: Methods*, *17*, 627–638. doi: doi:10.1002/lom3.10337

Hellerman, S. (1967). An updated estimate of the wind stress on the world ocean. *Mon. Wea. Rev*, *95*(9), 607–626.

Hench, J. L., Leichter, J. J., & Monismith, S. G. (2008). Episodic circulation and exchange in a wave-driven coral reef and lagoon system. *Limnology and Oceanography*, *53*(6), 2681–2694.

Herdman, L. M., Hench, J. L., & Monismith, S. G. (2015). Heat balances and thermally driven lagoon-ocean exchangeson a tropical coral reef system (moorea, french polynesia). *Journal of Geophysical Research: Oceans*, *120*(2), 1233–1252.

Koweek, D. A., Dunbar, R. B., Monismith, S. G., Mucciarone, D. A., Woodson, C. B., & Samuel, L. (2015). High-resolution physical and biogeochemical variability from a shallow back reef on ofu, american samoa: An end-member perspective. *Coral Reefs*, *34*(3), 979–991.

Kundu, P. K., Cohen, I. M., & Dowling, D. (2008). *Fluid mechanics 4th.* Elsevier.

Lentz, S. J., Davis, K. A., Churchill, J. H., & DeCarlo, T. M. (2017). Coral reef drag coefficients–water depth dependence. *Journal of Physical Oceanography*, *47*(5), 1061–1075.

Lindhart, M., Rogers, J. S., Maticka, S. A., Woodson, C. B., & Monismith, S. G. (2021). Wave modulation of flows on open and closed reefs. *Journal of Geophysical Research: Oceans*, *126*(4), e2020JC016645. doi: https://doi.org/10.1029/2020JC016645

Longuet-Higgins, M., & Stewart, R. (1964). Radiation stresses in water waves; a physical discussion, with applications. *Deep Sea Research and Oceanographic Abstracts*, *11*(4), 529-562.

Lowe, R. J., Falter, J. L., Monismith, S. G., & Atkinson, M. J. (2009). Wave-driven circulation of a coastal reef–lagoon system. *Journal of Physical Oceanography*, *39*(4), 873–893.

Lowe, R. J., Hart, C., & Pattiaratchi, C. B. (2010). Morphological constraints to wave-driven circulation in coastal reef-lagoon systems: A numerical study. *Journal of Geophysical Research: Oceans*, *115*(C9).

MacMahan, J. H., Thornton, E. B., & Reniers, A. J. (2006). Rip current review. *Coastal Engineering*, *53*(2-3), 191–208.

Maticka, S. (2019). *A tale of two reefs: Hydrodynamics of a fringing reef and a reef atoll* (Unpublished doctoral dissertation). Stanford University.

Mei, C. C., Stiassnie, M., & Yue, D. K.-P. (1989). *Theory and applications of ocean surface waves: Part 1: Linear aspects part 2: Nonlinear aspects.* World Scientific.

Monismith, S. G., Herdman, L. M., Ahmerkamp, S., & Hench, J. L. (2013). Wave transformation and wave-driven flow across a steep coral reef. *Journal of Physical Oceanography*, *43*(7), 1356–1379.

Monismith, S. G., Rogers, J. S., Koweek, D., & Dunbar, R. B. (2015). Frictional wave dissipation on a remarkably rough reef. *Geophysical Research Letters*, *42*(10), 4063–4071.

Munk, W. H., & Sargent, M. C. (1954). Adjustment of bikini atoll to ocean waves. *Geophysical Union*, *29*, 855-860.

Oliver, T. A., & Palumbi, S. R. (2009). Distributions of stress-resistant coral symbionts match environmental patterns at local but not regional scales. *Marine* *ecology progress series*, *378*, 93–103.

Péquignet, A.-C. N., Becker, J., Merrifield, M., & Boc, S. (2011). The dissipation of wind wave energy across a fringing reef at ipan, guam. *Coral Reefs*, *30*(1), 71–82.

Péquignet, A.-C. N., Becker, J. M., & Merrifield, M. A. (2014). Energy transfer between wind waves and low-frequency oscillations on a fringing reef, i pan, g uam. *Journal of Geophysical Research: Oceans*, *119*(10), 6709–6724.

Péquignet, A.-C. N., Becker, J. M., Merrifield, M. A., & Aucan, J. (2009). Forcing of resonant modes on a fringing reef during tropical storm man-yi. *Geophysical Research Letters*, *36*(3).

Pope, S. B. (2000). *Turbulent flows.* Cambridge University Press.

Raubenheimer, B., Guza, R., & Elgar, S. (1996). Wave transformation across the inner surf zone. *Journal of Geophysical Research: Oceans*, *101*(C11), 25589–25597.

Rogers, J. S., Maticka, S. A., Chirayath, V., Woodson, C. B., Alonso, J. J., & Monismith, S. G. (2018). Connecting flow over complex terrain to hydrodynamic roughness on a coral reef. *Journal of Physical Oceanography*, *48*(2018).

Rogers, J. S., Monismith, S. G., Fringer, O. B., Koweek, D. A., & Dunbar, R. B. (2017). A coupled wave-hydrodynamic model of an atoll with high friction: Mechanisms for flow, connectivity, and ecological implications. *Ocean Modelling*, *110*, 66-82. doi: https://doi.org/10.1016/j.ocemod.2016.12.012

Rosman, J. H., & Hench, J. L. (2011). A framework for understanding drag parameterizations for coral reefs. *Journal of Geophysical Research: Oceans*, *116*(C8).

Sheremet, A., Guza, R., Elgar, S., & Herbers, T. (2002). Observations of nearshore infragravity waves: Seaward and shoreward propagating components. *Journal of Geophysical Research: Oceans*, *107*(C8), 10–1.

Sous, D., Dodet, G., Bouchette, F., & Tissier, M. (2020). Momentum balance over a barrier reef. *Journal of Geophysical Research. Oceans*, *125*(2).

Sous, D., Tissier, M., Rey, V., Touboul, J., Bouchette, F., Devenon, J.-L., … Aucan, J. (2019). Wave transformation over a barrier reef. *Continental Shelf Research*, *184*, 66–80.

Storlazzi, C. D., Gingerich, S. B., van Dongeren, A., Cheriton, O. M., Swarzenski, P. W., Quataert, E., … others (2018). Most atolls will be uninhabitable by the mid-21st century because of sea-level rise exacerbating wave-driven flooding. *Science advances*, *4*(4), eaap9741.

Svendsen, I. A. (1984). Mass flux and undertow in a surf zone. *Coastal Engineering*, *8*(4), 347–365.

Symonds, G., Black, K. P., & Young, I. R. (1995). Wave-driven flow over shallow reefs. *Journal of Geophysical Research: Oceans*, *100*(C2), 2639–2648.

Taebi, S., Lowe, R. J., Pattiaratchi, C. B., Ivey, G. N., Symonds, G., & Brinkman, R. (2011). Nearshore circulation in a tropical fringing reef system. *Journal of Geophysical Research: Oceans*, *116*(C2).

Vetter, O., Becker, J. M., Merrifield, M. A., Pequignet, A.-C. N., Aucan, J., Boc, S. J., & Pollock, C. E. (2010). Wave setup over a pacific island fringing reef. *Journal of Geophysical Research: Oceans*, *115*(C12). doi: https://doi.org/10.1029/2010JC006455

Wiens, H. J., et al. (1962). *Atoll environment and ecology.* Yale University Press.

Wright, D. G., & Thompson, K. R. (1983). Time-averaged forms of the nonlinear stress law. *Journal of Physical Oceanography*, *13*(2), 341–345.

Yao, Y., Huang, Z., Monismith, S. G., & Lo, E. Y. (2012). 1dh boussinesq modeling of wave transformation over fringing reefs. *Ocean Engineering*, *47*, 30-42. doi: https://doi.org/10.1016/j.oceaneng.2012.03.010

Zhang, Z., Falter, J., Lowe, R., & Ivey, G. (2012). The combined influence of hydrodynamic forcing and calcification on the spatial distribution of alkalinity in a coral reef system. *Journal of Geophysical Research: Oceans*, *117*(C4).

Zhang, Z., Falter, J., Lowe, R., Ivey, G., & McCulloch, M. (2013). Atmospheric forcing intensifies the effects of regional ocean warming on reef-scale temperature anomalies during a coral bleaching event. *Journal of Geophysical Research: Oceans*, *118*(9), 4600–4616.

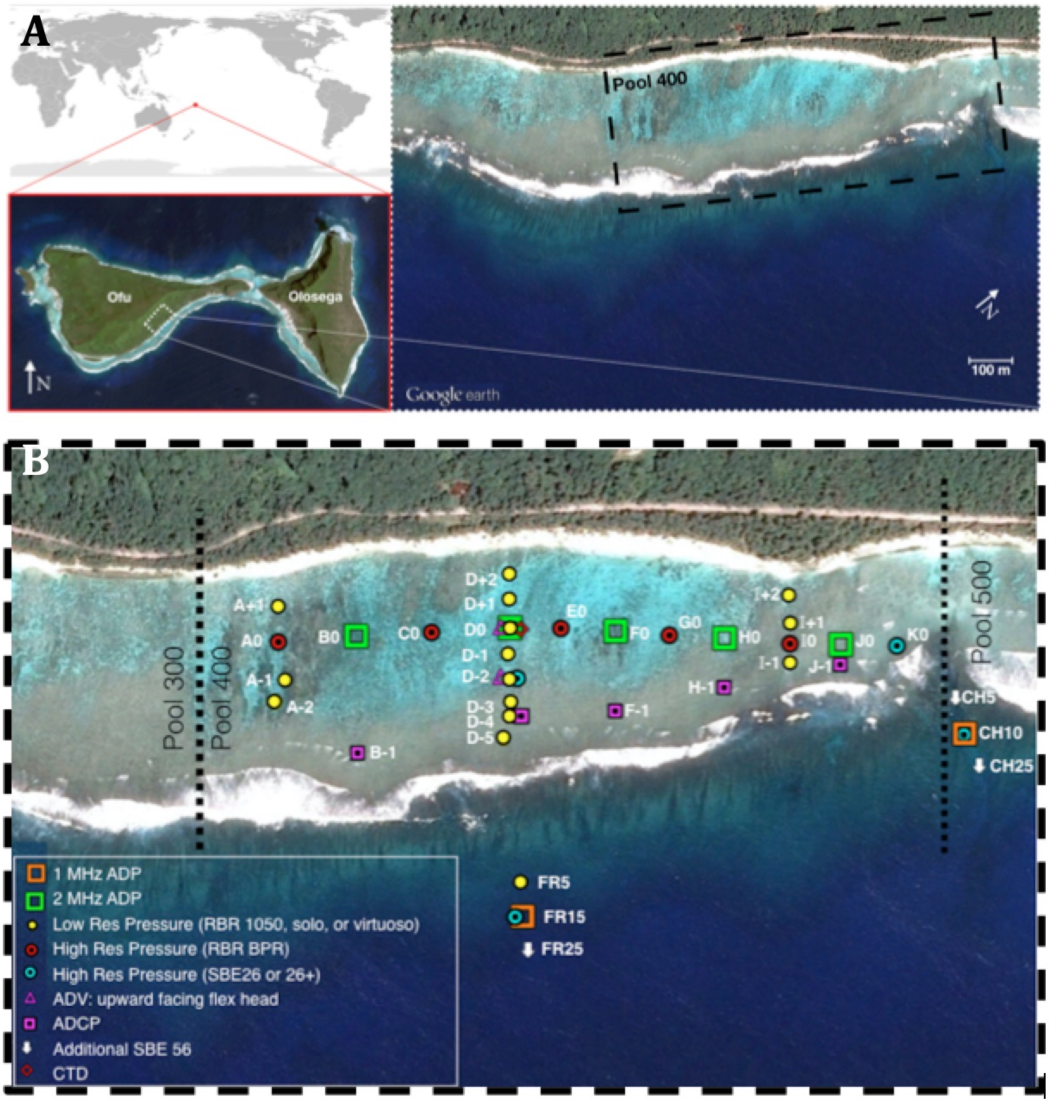

Figure 1. a) Ofu, American Samoa. Pool 400 (dashed box) denotes study focus. b) March 2017 deployment; dashed lines are approximate separation points of pools

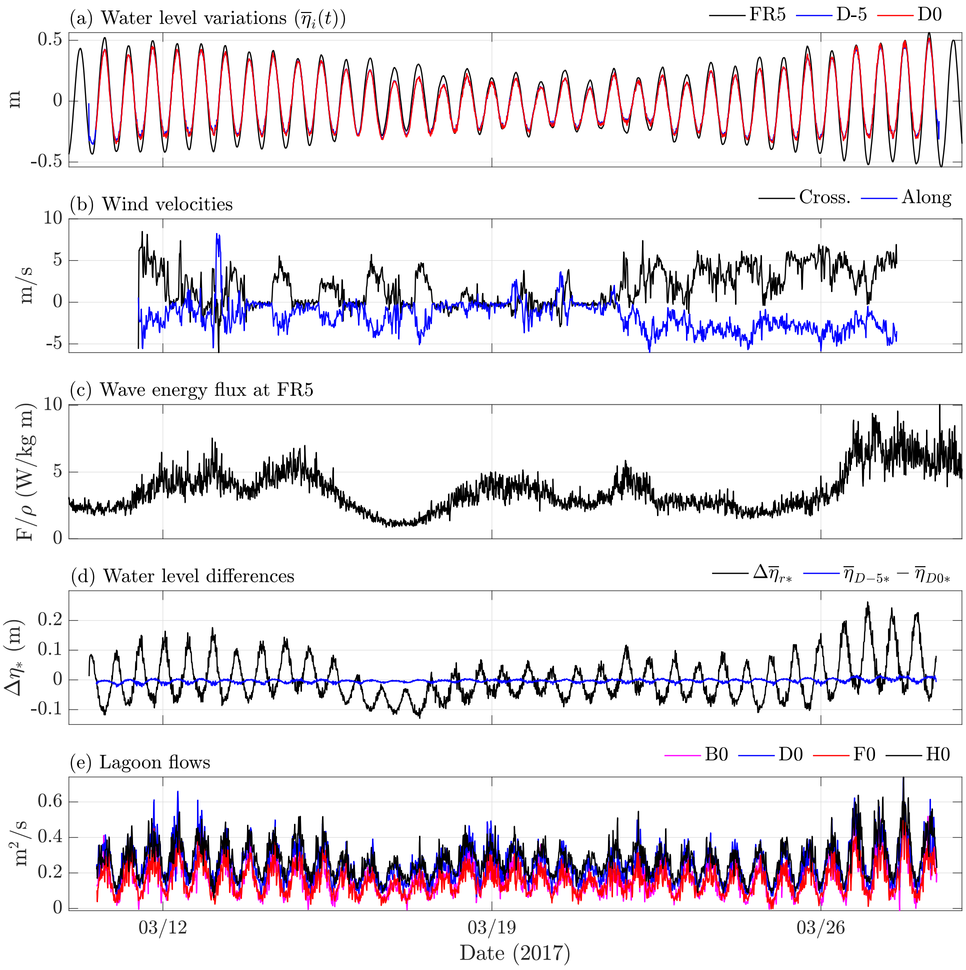

Figure 2. Field Conditions during study. a) Water level variations; b) Wind velocities ; c) Wave energy flux on the forereef (FR5); d) Water level differences fore-reef to reef flat ($\Delta\overline{\eta}_{r*} = \overline{\eta}_{D-5*} - \overline{\eta}_{FR5*}$) and reef flat to lagoon ($\overline{\eta}_{D0*} - \overline{\eta}_{D-5*}$) ; e) Lagoon alongshore transports (positive toward channel)

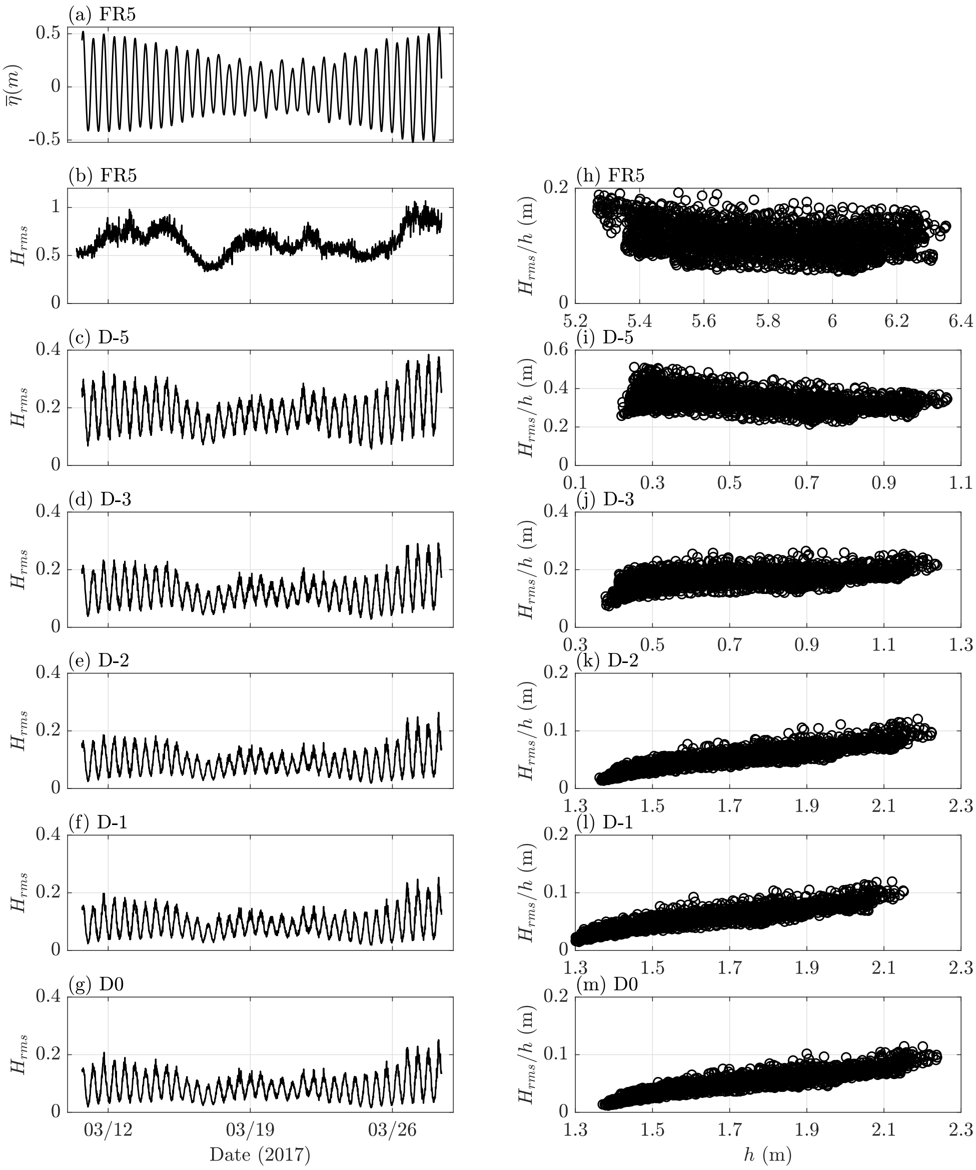

Figure 3. (a) Depth at FR5; (b)-(g) RMS wave heights on the D transect line; (h) to (m) RMS wave height for normalized by depth as a function of depth for the same stations shown in (a) to (e).

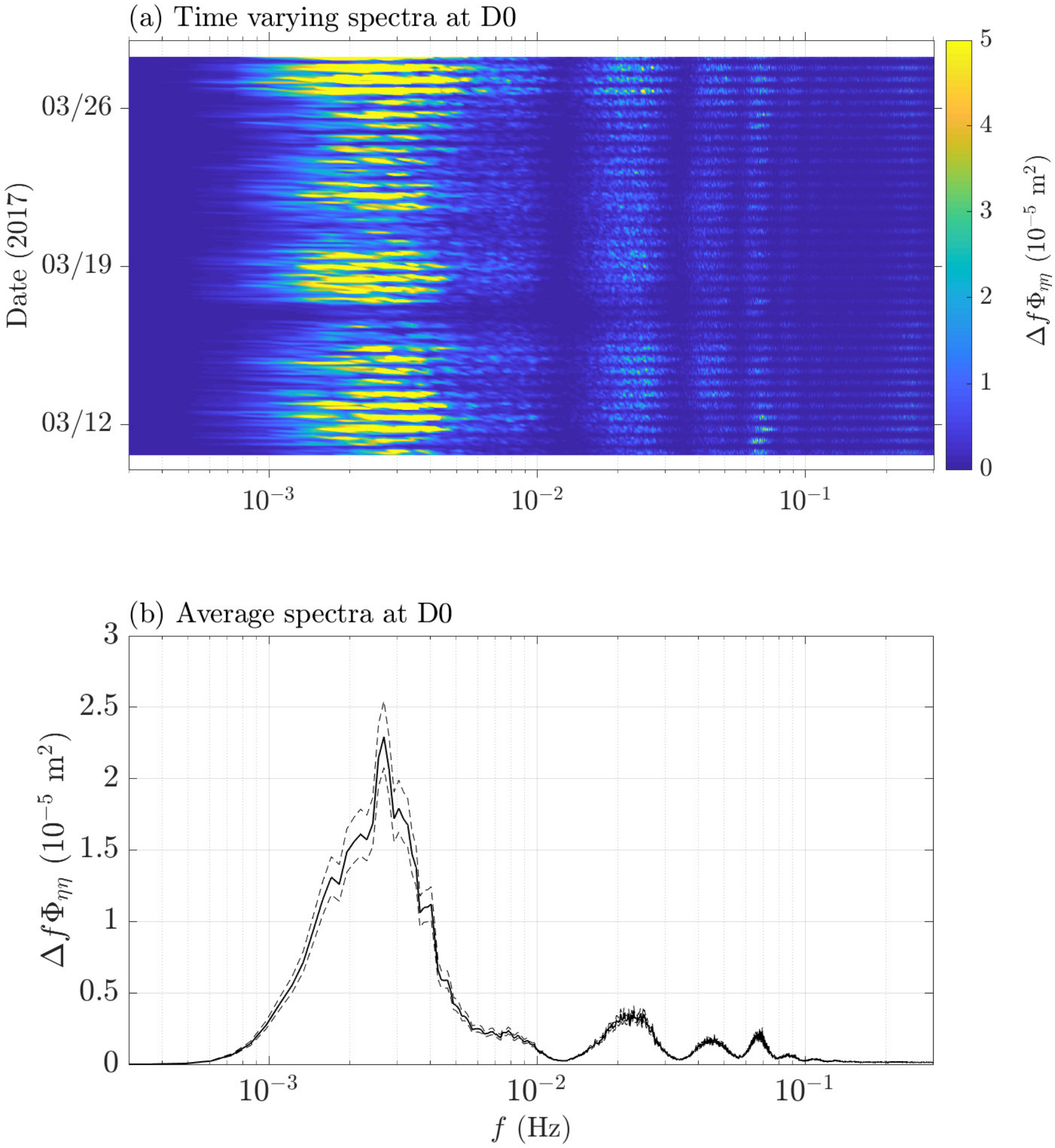

Figure 4. (a) Time varying spectra in the Ofu lagoon (D0) (b) Average for entire record of the spectra seen in (a). In (b), the dashed lines show the 95 % confidence intervals.

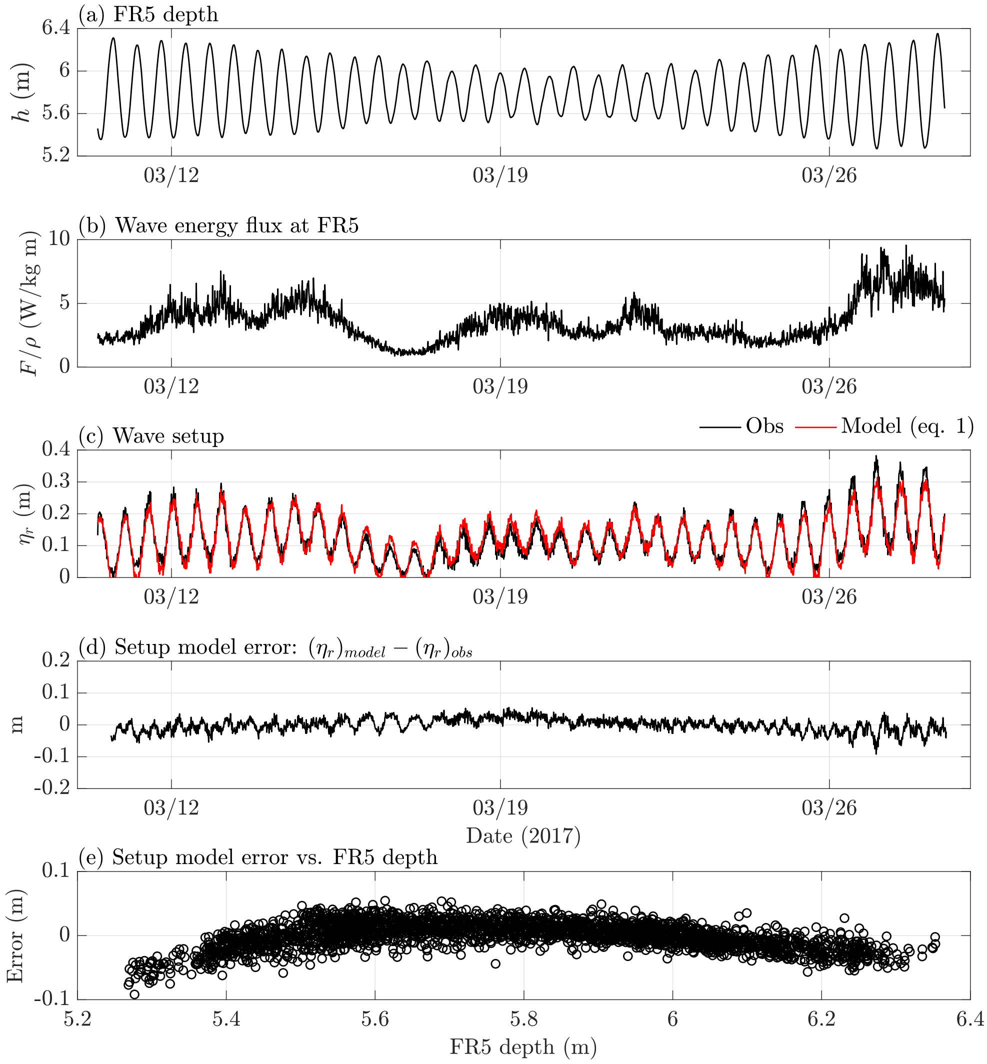

Figure 5. (a) Depth on fore-reef (FR5); (b) Wave energy flux at FR5; (c) Observed and modeled setups on reef flat; (d) Error in predicted setup as a function of time; (e) Error in predicted setup as a function of fore-reef depth.

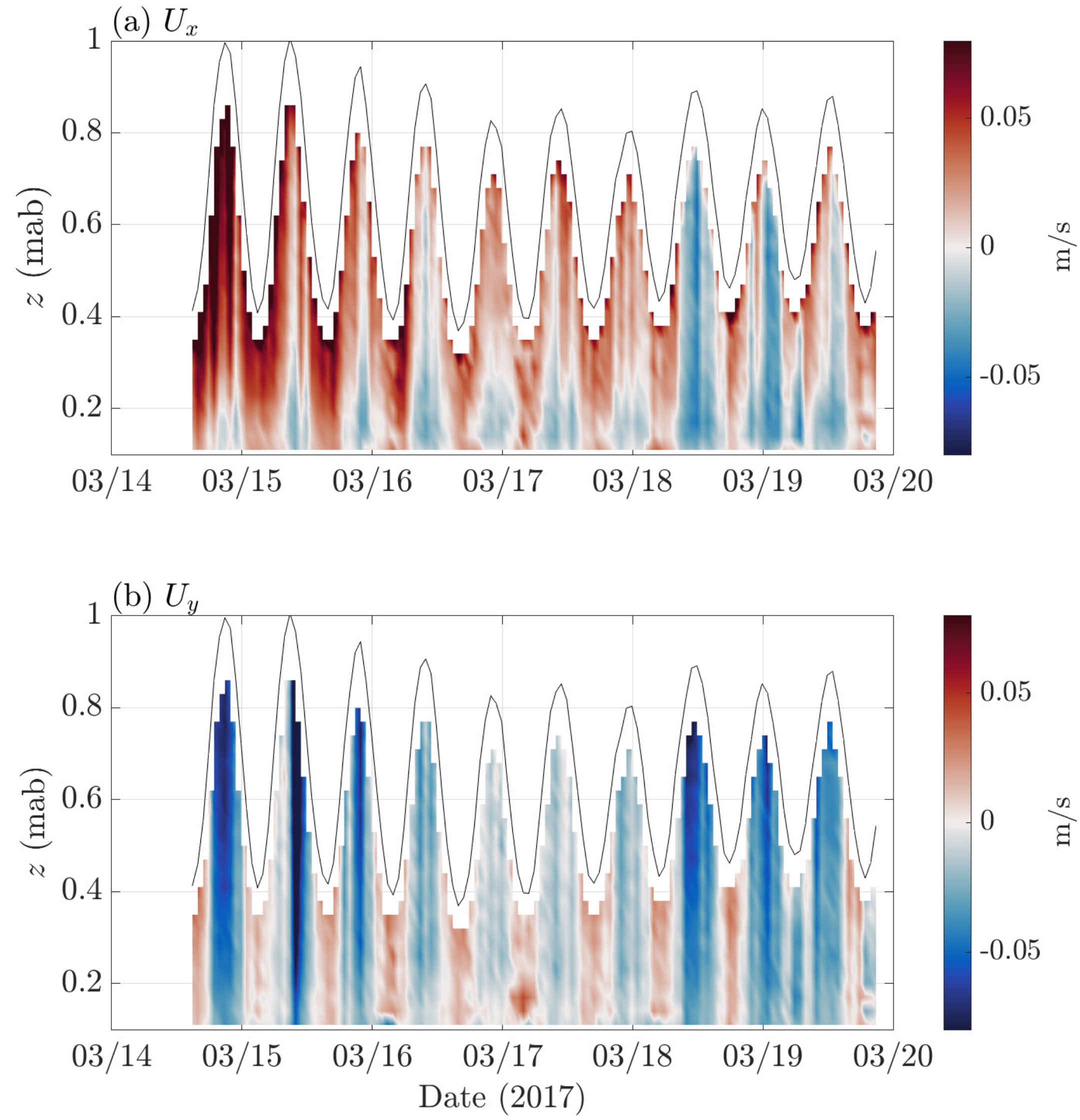

Figure 6. vADCP measured velocities at D-4: (a) Cross-reef flows (+ve onshore); (b) Along-reef flows (-ve directed towards channel)

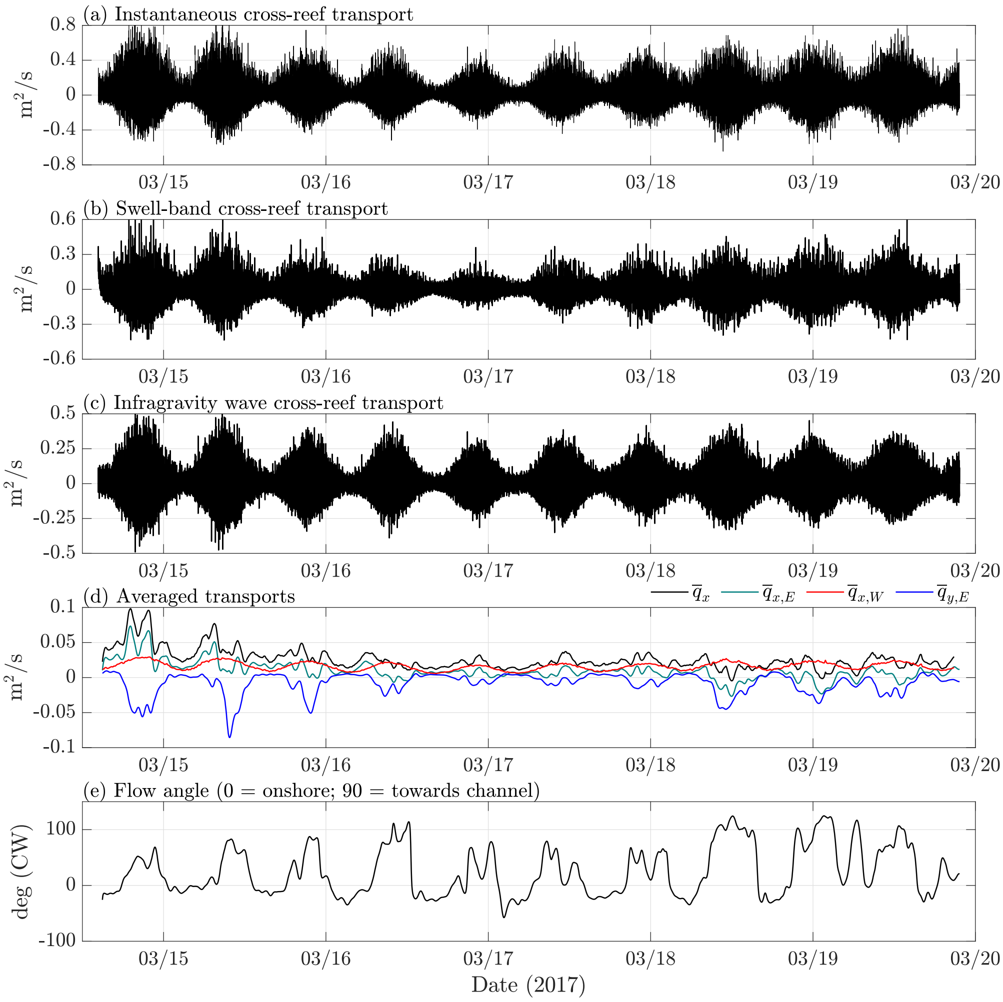

Figure 7. vADCP transports measured at D-4: (a) q; (b)Instantaneous swell band wave transport; (c) Instantaneous infragravity wave transport; (d)Wave averaged transports in the cross-shore (x) and along-shore directions (y); (d) angle of the wave-averaged flow relative to the x direction (+ve CW)

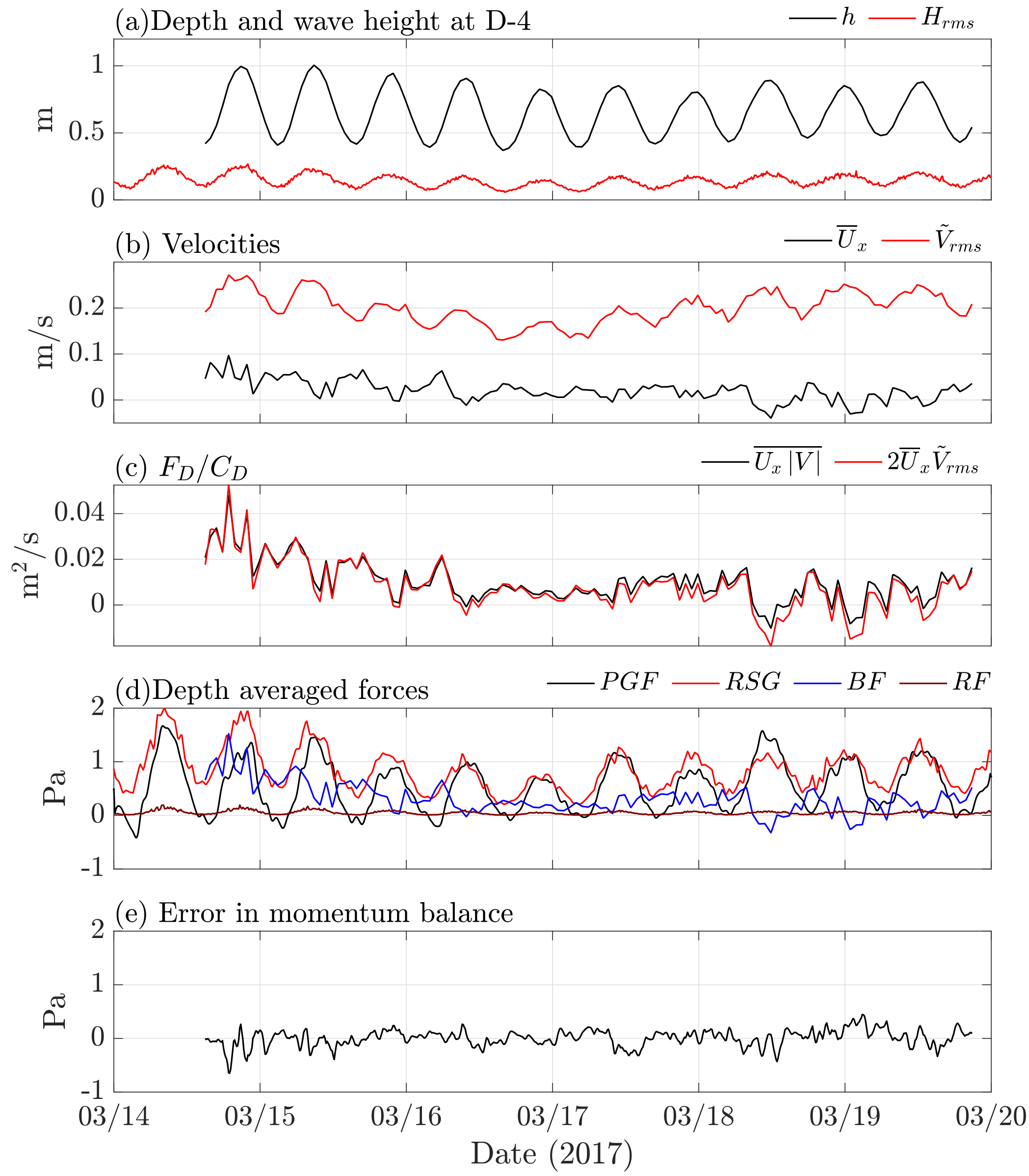

Figure 8. Reef flat dynamics: (a) Depth and rms wave height; (b) Wave-averaged cross-reef flow and rms wave velocity; (c) Drag/ρC_D: exact and the model of Wright and Thompson (1983); (d) Forces on the reef flat - individual terms are defined in eq.10; (e) Error as given by eq. 17.

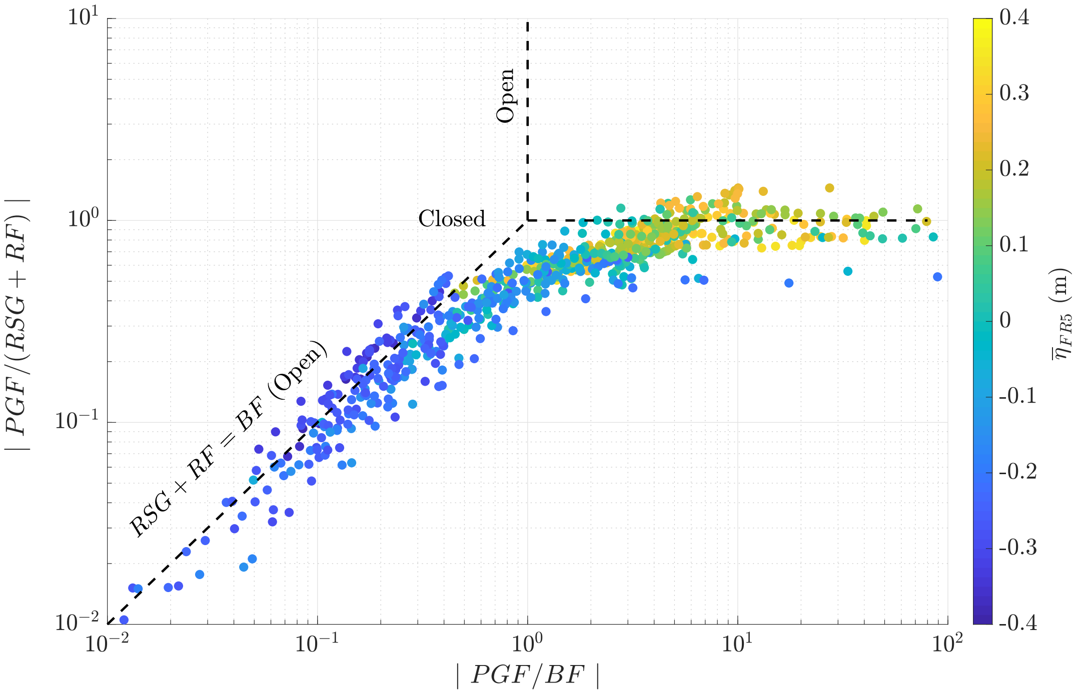

Figure 9. Reef flat dynamics: Force balances as a function of depth. The dashed lines indicate different regimes of the force balance defined by eq.10.

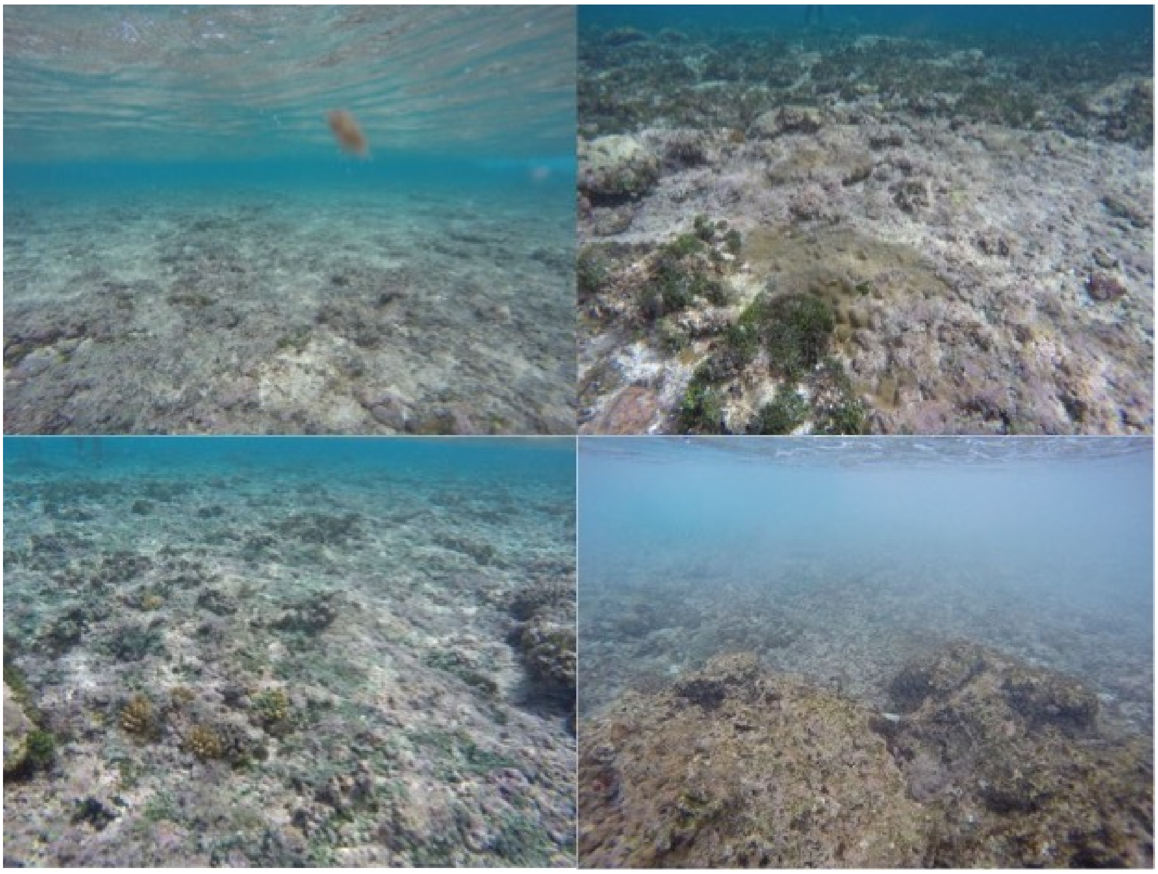

Figure 10. Sample images of Ofu reef flat showing low relief topography and sparse coral colonies. The largest features in these photos are roughly 10 cm high.

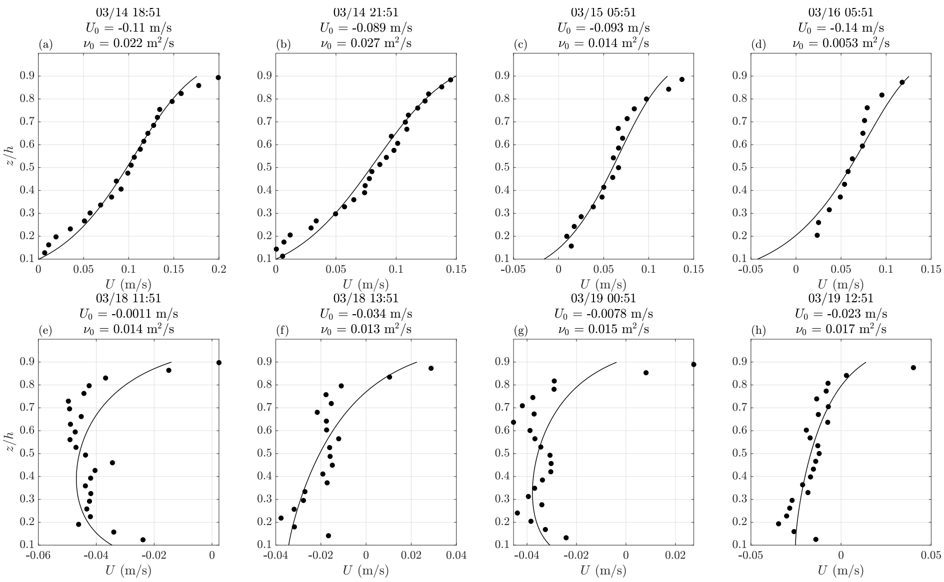

Figure 11. Vertical structure of flows on the reef flat dynamics: (•) observations and (—) Svendsen's (1984) model. In each case, times, and values of U_0 and ν_0 are given.

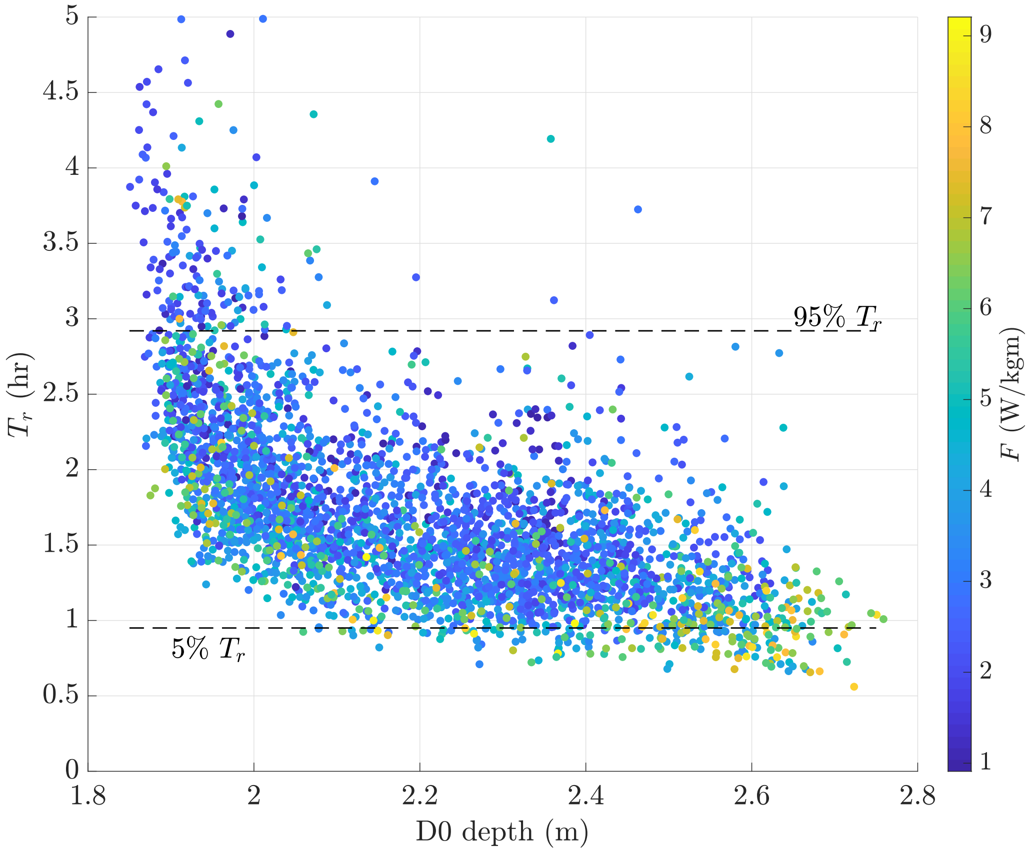

Figure 12. Residence time scale estimated from the velocity measured at D0. The two dashed lines indicate the 5% and 95% residence times based on the entire record.

Station	**Location**	**Depth (m)**	**Instruments**	**Sampling**
D0	Lagoon	1.72	RBR Solo Pressure	2 Hz continuous
			2 MHz Nortek ADP	Profile: 3' intervals; 0.15 m bins Waves: Burst 30'; 1024 samples @ 2 Hz
D-1, D-2, D-3, D-5	Reef flat	1.6, 1.4, 0.72, 0.55	RBR Solo Pressure	2 Hz continuous
D-4	Reef flat	0.65	TRDI vADCP	0.33 Hz; 0.03 m bins; 1st bin: 0.11 mab
FR5	Forereef	5.8	RBR Solo Pressure	2 Hz continuous
FR15	Forereef	15.4	Seabird SBE26+ Pressure	Tides: 10' (1' avg.); Waves: Burst 30': 1024 samples @ 2Hz
			1 MHz Nortek ADP	Profiles: 5' intervals; 0.5 m bins Waves: Burst 30': 1024 samples @ 1 Hz
H-1	Reef flat	0.59	TRDI vADCP	0.33 Hz; 0.03 m bins 1st bin: 0.11 mab

Table 1. Wave and flow measurements Ofu March 2017. Instruments shown are ones referred to in this paper. Details for the complete set of instruments shown in Fig. 1 can be found in Maticka (2019)

.